Molecular BioSystems

RSC Publishing

PAPER

View Article Online
View Journal | View Issue

Cite this: *Mol. BioSyst.*, 2013, **9**, 732

Quantitative global phosphoproteomics of human umbilical vein endothelial cells after activation of the Rap signaling pathway†

Lars A. T. Meijer,‡[a] Houjiang Zhou,‡[bc] On Ying A. Chan,‡[a] A. F. Maarten Altelaar,[bc] Marco L. Hennrich,[bc] Shabaz Mohammed,[bc] Johannes L. Bos*[a] and Albert J. R. Heck*[bc]

Received 17th November 2012,
Accepted 21st January 2013

DOI: 10.1039/c3mb25524g

www.rsc.org/molecularbiosystems

The small GTPase Rap1 is required for proper cell–cell junction formation and also plays a key role in mediating cAMP-induced tightening of adherens junctions and subsequent increased barrier function of endothelial cells. To further study how Rap1 controls barrier function, we performed quantitative global phosphoproteomics in human umbilical vein endothelial cells (HUVECs) prior to and after Rap1 activation by the Epac-selective cAMP analog 8-pCPT-2′-*O*-Me-cAMP-AM (007-AM). Tryptic digests were labeled using stable isotope dimethyl labeling, enriched with phosphopeptides by strong cation exchange (SCX), followed by titanium(IV) immobilized metal affinity chromatography (Ti^{4+}-IMAC) and analyzed by high resolution mass spectrometry. We identified 19 859 unique phosphopeptides containing 17 278 unique phosphosites on 4594 phosphoproteins, providing the largest HUVEC phosphoproteome to date. Of all identified phosphosites, 220 (~1%) were more than 1.5-fold up- or downregulated upon Rap activation, in two independent experiments. Compatible with the function of Rap1, these alterations were found predominantly in proteins regulating the actin cytoskeleton, cell–cell junctions and cell adhesion.

Introduction

To regulate the passage of plasma components and circulating cells into the surrounding tissue, blood vessels are lined with a monolayer of endothelial cells. Fluids, solutes, macromolecules and activated immune cells pass through or between endothelial cells *via* transcellular or paracellular pathways, respectively. Aberrant functioning of the endothelial barrier may lead to several pathological conditions including chronic inflammation, sepsis, ischemia, atherosclerosis and diabetes. Cell–cell contacts play a crucial role in maintaining the barrier function by regulating the intercellular space and linking the cortical actin networks of neighboring cells. In endothelial cells, the endothelial barrier function is mainly attributed to the adherens junctions, as the tight junctional structure is less defined and underdeveloped.[1,2]

An important regulator of the endothelial barrier function is the Ras-like small G-protein Rap. Similar to all G-proteins, Rap cycles between an inactive GDP bound and an active GTP bound state. This cycling is further regulated by guanine nucleotide exchange factors (GEFs) that exchange GDP for the cellular more abundant GTP, and GTPase activating proteins (GAPs) that catalyze the hydrolyzation of GTP.[3] Rap is regulated by multiple GEFs that ensure spatial and temporal regulation of Rap activation (reviewed in ref. 4). One of the most studied RapGEFs is the exchange protein directly activated by cAMP (Epac), which exists in two isoforms Epac1 and Epac2, with Epac1 being the predominant form in endothelial cells.[5,6] Studies in the past have shown that the activation of Epac with cAMP or the Epac-specific cAMP analogue 8-pCPT-2′-*O*-Me-cAMP (hereafter referred to as 007)[7] increases the impedance with which a monolayer of endothelial cells opposes an electrical current and which is a measure for endothelial barrier function.[8–11] Morphologically this is accompanied by a tightening or straightening

[a] *Molecular Cancer Research, Centre for Biomedical Genetics and Cancer Genomics Centre, University Medical Center Utrecht, Universiteitsweg 100, 3584 CG Utrecht, The Netherlands. E-mail: j.l.bos@umcutrecht.nl*
[b] *Biomolecular Mass Spectrometry and Proteomics, Utrecht Institute for Pharmaceutical Sciences and Bijvoet Center for Biomolecular Research, Utrecht University, Padualaan 8, 3584 CH Utrecht, The Netherlands. E-mail: a.j.r.heck@uu.nl*
[c] *Netherlands Proteomics Centre, Padualaan 8, 3584 CH Utrecht, The Netherlands*

† Electronic supplementary information (ESI) available. See DOI: 10.1039/c3mb25524g

‡ These authors contributed equally to this work.

of the cell junctions and actin rearrangements, resulting in an increase in junctional actin.[8]

Recently, the RapGEFs PDZ-GEF1 and PDZ-GEF2 have been implicated in regulating the basal barrier function as opposed to the cAMP induced barrier function, which is Epac1-dependent.[12] Depletion of PDZ-GEF1 and 2 destabilizes the cell junctions and is evidenced by a decrease in impedance and an increase in cell motility, a phenotype similar to Rap1 depletion. Depletion of Epac1 does not affect the basal impedance but inhibits the cAMP induced barrier function only. Importantly, activation of Rap through Epac1 is able to rescue the depletion of PDZ-GEF1 and 2, as it overcomes the initial junction instability.

In the past, several effector proteins have been reported to function downstream of Rap1 in the endothelial barrier function. AF6 (MLLT4/afadin) has been proposed to influence the barrier function directly *via* its interaction with the adherens junctions.[13,14] Activation of Rap1 enhances the interaction of AF6 with p120 catenin, which in turn increases the binding between the adherens junction proteins p120 catenin and E-cadherin. The Rap1 effector Krev interaction trapped protein 1 (KRIT/CCM1) has been proposed to regulate barrier function *via* its inhibitory effect on RhoA and cell contractility.[15,16] In addition, the small G-protein Rac1 has been implicated to function downstream of Rap1 in regulation of the barrier function *via* the RacGEFs VAV2 and T-lymphoma invasion and metastasis-inducing protein (TIAM).[13,17] Rap1 affects the localization of VAV2, which in turn regulates the activation of Rac1.

Here, we sought to get a global view of protein phosphorylation events that occur downstream of Rap signaling in primary endothelial cells. Protein phosphorylation is thought to be one of the most abundant posttranslational modifications. This highly dynamic and reversible modification is governed by the actions of a plethora of protein kinases and phosphatases. In mammalian cells, at least 70% of all proteins become phosphorylated during their lifetime[18] and the crucial role of protein phosphorylation in many cellular processes is well established.[19] To study *in vivo* protein phosphorylation dynamics on a global scale, a number of tools have been developed over the last few years. As regulatory phosphorylations predominantly occur at a small fraction of the total pool of a particular protein, which is often itself present at low stoichiometric levels, it is a challenging task to identify these phosphorylation sites in a complex cell lysate.

In this study we combine several state-of-the-art quantitative phosphoproteomic methods, including the recently developed titanium(IV) immobilized metal affinity chromatography (Ti^{4+}-IMAC) affinity enrichment,[20] to globally profile phosphorylation-based signaling events in response to Rap activation in primary endothelial cells. We use the Epac-selective cAMP analog 007-AM (8-pCPT-2′-*O*-Me-cAMP-AM), a modified version of 007 with increased membrane permeability,[21] to activate endogenous Epac in human umbilical vein endothelial cells (HUVECs). These cells were depleted of both PDZ-GEF1 and 2 to maximize the stimulatory window.[12] Tryptic digests of 007-AM treated and mock treated HUVECs were labeled with either light or intermediate stable isotope dimethyl labels. Subsequently, the peptide mixtures were mixed in a 1 : 1 ratio, enriched for phosphopeptides using strong cation exchange (SCX)[22,23] and Ti^{4+}-IMAC and analyzed by high resolution and high accuracy liquid chromatography–mass spectrometry/mass spectrometry (LC-MS/MS) using a data-dependent decision tree (ddDT) logic[24] and collision-induced dissociation–multistage activation (CID-MSA).[25] This resulted in the identification of 19 859 unique phosphopeptides containing 17 278 unique phosphosites on 4594 phosphoproteins, by far the largest phosphoproteome dataset of endothelial cells to date. Upon Rap activation, only a small fraction (~1%), namely 220 of the identified phosphosites, is more than 1.5-fold up- or downregulated in two independent experiments. Kinase predictions and amino acid overrepresentation analyses reveal that phosphorylations downstream of Rap that are primarily imposed by basophilic kinases and phosphosites that are downregulated are target sites of proline-directed kinases, indicating a shift from one kinase class to another. Pathway, gene ontology (GO) term and protein network analyses indicate that Rap-induced phosphorylations occur on proteins involved in actin and microtubule skeletal rearrangements, cell–cell junction regulation and cell–substratum adhesion. We conclude that in HUVECs Rap activation affects the phosphorylation status of various proteins, some of which have previously been implicated in endothelial cell permeability. Moreover, we disclose numerous novel potential regulatory phosphorylation sites that may serve as the foundation for future investigations.

Materials and methods

Cell culture, ECIS measurements and immunofluorescence

Human umbilical vein endothelial cells (HUVECs) (Lonza) were cultured in EBM-2 culture medium supplemented with EGM-2 SingleQuots (hEGF, hydrocortisone, fetal bovine serum, VEGF, hFGF-B, R3-IGF-1, ascorbic acid, GA-1000, heparin) (Lonza) on dishes coated with 5 μg ml^{-1} home purified human fibronectin. HUVECs were transfected with 50 nM ON-TARGETplus SMARTpools (Dharmacon Inc.) against PDZ-GEF1 and PDZ-GEF2 using Dharmafect-1 (Dharmacon Inc.) according to the manufacturer's guidelines.

HUVECs were plated onto L-cysteine reduced, fibronectin coated 8W10E electrode arrays (1×10^5 cells per well) (Applied Biophysics) 48 hours after transfection and grown to confluency overnight. Electrical impedance was measured in real-time at 4000 Hz using electric cell–substrate impedance sensing (ECIS) (Applied Biophysics).[26] HUVECs were stimulated with 8-pCPT-2′-*O*-Me-cAMP-AM (007-AM) at a final concentration of 0.1 μM (Biolog Life Sciences).

For immunofluorescence HUVECs were fixed in 3.8% formaldehyde, permeabilized in 0.1% Triton X-100 and blocked in 2% BSA. Cells were stained by incubation with the anti-β-catenin (BD Biosciences) antibody, and the secondary antibodies alexa fluor 488 phalloidin and anti-mouse alexa fluor 568 (Invitrogen). Cells were examined using an Axioskop2 mot plus microscope (Zeiss) with a 40× or 100× Plan APO objective lens, and images were acquired using an Axiocam CCD camera.

Sample preparation

HUVECs were transfected with 50 nM ON-TARGETplus siRNA SMARTpools (Dharmacon Inc.) targeted against PDZ-GEF1 and

PDZ-GEF2 using Dharmafect-1 (Dharmacon Inc.) three days prior to harvesting. One day before harvesting, cells were replated and grown until confluence was reached. Cells were maintained in four populations of which two were used for the 'Forward' experiment and two for the 'Reverse' experiment. When applicable, cells were stimulated for 15 minutes with 007-AM at a final concentration of 1 μM. Subsequently, cell lysis was performed by harvesting the cells in lysis buffer (50 mM ammonium bicarbonate, 8 M urea, 2 M thiourea, 1 tablet 10 ml^{-1} Complete Mini EDTA-free Protease Inhibitor Cocktail (Roche), 1 tablet 10 ml^{-1} PhosSTOP Phosphatase Inhibitor Cocktail (Roche)) and subjecting them to ultrasonication. Cell debris was removed by centrifugation at 20 000 × g for 15 min at 4 °C, after which the supernatant was transferred to a new reaction tube. Protein concentrations were determined using a Bradford assay (Bio-Rad). For each condition 2 mg of protein was reduced using 2 mM dithiothreitol and incubation for 30 min at 56 °C and subsequently alkylated using 4 mM iodoacetamide and incubation for 30 min at room temperature in the dark. Next, the initial digestion was performed by adding Lys-C (WAKO) at an enzyme/protein ratio of 1 : 75 and incubation for 4 h at 37 °C. The sample was diluted 4-fold to a final urea concentration of 2 M using 50 mM ammonium bicarbonate buffer. The final digestion was performed by adding Trypsin Gold, Mass Spectrometry Grade (Promega), at an enzyme/protein ratio of 1 : 100 and incubation overnight at 37 °C. Formic acid (FA) was added to a final concentration of 10%, after which the peptide mixtures were desalted using Sep-Pak Vac C18 cartridges (3 cc/200 mg, Waters). Subsequently, on-column stable isotope dimethyl labeling was performed as described previously.[27] For the 'Forward' experiment, the peptides from the unstimulated control sample were labeled with light dimethyl labels and those from the 007-AM stimulated sample with intermediate dimethyl labels. Conversely, for the 'Reverse' experiment the 007-AM stimulated sample was labeled with light dimethyl labels and the unstimulated control sample with intermediate dimethyl labels. Finally, the eluates corresponding to either the 'Forward' or 'Reverse' experiment were mixed in a 1 : 1 ratio, dried *in vacuo* and stored at −20 °C. Label incorporation and mixing accuracy were assessed by LC-MS/MS.

SCX chromatography for peptide fractionation

The mixture of dimethyl labeled peptides with a 1 : 1 ratio were reconstituted in 10% FA and loaded onto a C18 cartridge (Aqua, Phenomenex) using an Agilent 1100 HPLC system. The flow rate applied was 100 μL min^{-1} using 0.05% FA (pH 2.7) as solvent. Peptides were eluted from the C18 cartridge with 80% acetonitrile (ACN) containing 0.05% FA (pH 2.7) onto a Polysulfoethyl A column (200 × 2.1 mm) (PolyLC) for 10 min at the same flow rate. Separation of peptides was performed using a nonlinear 65 min gradient: from 0 to 10 min, 100% solvent A (5 mM KH_2PO_4, 0.05% FA, 30% ACN, pH 2.7); from 10 min to 15 min, to 26% solvent B (5 mM KH_2PO_4, 0.05% FA, 30% ACN, 350 mM KCl, pH 2.7); from 15 min to 40 min, to 35% solvent B; and from 40 to 45 min, to 60% solvent B. At 49 min, the concentration of solvent B was 100%. The column was subsequently washed for 6 min with 100% solvent B and finally equilibrated with 100% solvent A for 9 min. The flow rate applied during the SCX gradient was 300 μL min^{-1}. Fractions were collected every minute for 40 min. After combing a few neighbor 'blank' fractions based on the recorded UV graph, a total of 33 fractions were desalted using Sep-Pak Vac C18 cartridges (3 cc/200 mg, Waters). Finally, the eluted peptides were equally divided over two tubes, dried *in vacuo* and stored at −20 °C for phosphopeptide enrichment and protein analysis.

Phosphopeptide enrichment

Ti^{4+}-IMAC material was prepared and used essentially as previously described by us.[20,28] The prepared Ti^{4+}-IMAC beads were loaded onto GELoader tips (Eppendorf) using a C8 plug to approximately 1–2 cm length of material. The enrichment procedure for all SCX fractions was as follows: the Ti^{4+}-IMAC material was pre-equilibrated two times with 30 μL of Ti^{4+}-IMAC loading buffer (80% ACN, 6% trifluoroacetic acid (TFA)). Next, each SCX fraction was resuspended in 80 μL of loading buffer and loaded onto the equilibrated GELoader tips. Then the Ti^{4+}-IMAC material was washed with 40 μL wash buffer A (50% ACN, 0.5% TFA, 200 mM NaCl) and subsequently with 40 μL wash buffer B (50% ACN, 0.1% TFA). Bound peptides were first eluted by 30 μL of 10% ammonia into 30 μL of 10% FA. Finally, the remainder of the peptides was eluted with 4 μL of (80% ACN, 2% FA). The collected eluate was further acidified by adding 6 μL of 100% FA and subsequently stored at −20 °C for LC-MS/MS analysis.

Mass spectrometry

The enriched peptides from the dimethyl labeled samples were subjected to a reversed phase nano-LC-MS/MS analysis consisting of an Agilent 1200 series HPLC system (as described before ref. 29) connected to an LTQ-Orbitrap Velos mass spectrometer equipped with an electron transfer dissociation (ETD) source (Thermo Fisher Scientific). The HPLC system was equipped with a 20 mm × 100 μm ReproSil-Pur 120 C18-AQ (3 μm bead size, Dr Maisch) trapping column (packed in-house) and a 400 mm × 50 μm ReproSil-Pur 120 C18-AQ (3 μm bead size, Dr Maisch) analytical column (packed in-house). Mobile phase solvents consisted of 0.1 M acetic acid in double distilled water (solvent C) and 0.1 M acetic acid in 80% ACN (solvent D). Depending on sample complexity we used a specific LC method: for samples of lower complexity we used a 120 min method and for samples of higher complexity a 180 min method. 120 min LC method: 100% solvent C for 10 min (trapping and washing, flow rate: 5 μL min^{-1}); 10–25% solvent D in 57 min; 25–50% solvent D in 25 min; 50–100% solvent D in 2 min; 100% solvent D for 3 min; 100% solvent C for 23 min. 180 min LC method: 100% solvent C for 10 min (trapping and washing, flow rate: 5 μL min^{-1}); 10–25% solvent D in 107 min; 25–50% solvent D in 35 min; 50–100% solvent D in 2 min; 100% solvent D for 3 min; 100% solvent C for 23 min. During the elution stage, the flow rate was passively split from 0.60 mL min^{-1} to 100 nL min^{-1}. Nanospray was achieved using a distally gold-coated fused silica emitter (360 μm o.d., 20 μm i.d., 10 μm tip i.d.; pulled and coated in-house)

set to an ion spray voltage of 1.7 kV. The LTQ Orbitrap Velos instrument was operated in positive ion mode and in data-dependent acquisition mode to automatically switch between MS and MS/MS. Survey full-scan MS spectra were acquired from 350 to 1500 *m*/*z* in the Orbitrap analyzer with a resolution of 30 000 at 400 *m*/*z* after accumulation to a target value of 500 000 in the linear ion trap (LTQ). Charge state screening was enabled and precursors with an unknown charge state or a charge state of 1+ were excluded from fragmentation. Precursor ions with a charge state of 2+ or higher were fragmented by (higher-energy collisional dissociation) HCD or ETD under control of an in-house developed data dependent decision tree.[24] For internal mass calibration, the 445.120025 ion was used as lock mass with a target lock mass abundance of 0%. In addition, a collision-induced dissociation–multistage activation (CID-MSA) methodology[25] in combination with the 180 min LC method was employed for the analysis of the fractions containing the 'neutral phosphopeptides'.[20] Precursor ion scanning was achieved as described above; however, spectra were acquired in the Orbitrap analyzer with a resolution of 60 000 at 400 *m*/*z*. The normalized collision energy was set to 35% and the threshold value for triggering an MS/MS event was set to 500 counts. If a neutral loss of 98 or 49 *m*/*z* was detected, an additional activation step was carried out as described in ref. 25. Dynamic exclusion was enabled (exclusion list size 500, exclusion duration 90 s).

For the proteome analysis, a small portion of seven SCX fractions with charge '2+' and '3+' were separated with the 180 min LC method using an LTQ Orbitrap XL ETD mass spectrometer (Thermo Scientific). For survey full-scan MS spectra the mass spectrometer was operated as described for the CID-MSA method. The five most intense peaks at a threshold of above 500 counts were fragmented in the linear ion trap using a CID/ETD decision tree[30] at a target value of 30 000. The normalized collision energy for CID was set to 35%. The ETD reagent target value was set to 100 000 and the reaction time to 50 ms. Supplemental activation was enabled for ETD.[31] Dynamic exclusion settings were identical to those of the CID-MSA method.

Data analysis

All MS data were processed with Proteome Discoverer (version 1.3, Thermo Scientific) with standardized workflows. In detail, peak lists of CID, HCD and ETD fragmentation spectra were generated with Proteome Discoverer with a signal-to-noise threshold of 3. The ETD non-fragment filter was also taken into account as precursor peak removal within 4 Da, charge-reduced precursor removal within 2 Da, and removal of known neutral losses from charge-reduced precursor within 2 Da (the maximum neutral loss mass was set to 120 Da). All generated peak lists were searched against a Swissprot database (version 56.2, taxonomy filter was set to *Homo sapiens*) using Mascot software (version 2.3.02, Matrix Science). The database search was performed with the following parameters: trypsin cleavage specificity was selected, allowing two missed cleavages. The initial precursor mass tolerance was set at ±50 ppm and product ion tolerance was set at ±0.6 Da for ETD or CID LTQ fragment ions and ±0.05 Da for HCD and ETD FT fragment ions. Carbamidomethylation of cysteines was set as fixed modification, whereas oxidation of methionines, dimethylation and dimethylation:2 H(4) of lysines and protein N-termini were set as variable modifications. For the phosphoproteomic analysis phosphorylation of serine, threonine and tyrosine were set as variable modifications. The fragment ion type was specified as electrospray ionization FTMS-ECD, ETD-TRAP, ESI-TRAP and ESI-QUAD-TOF for the corresponding mass spectra. A decoy database search was enabled. For phosphorylation site localization we used the PhosphoRS algorithm,[32] which is integrated in Proteome Discoverer 1.3. For peptide quantitation, a dimethyl-based quantitation method with a mass precision requirement of 2 ppm for consecutive precursor measurements was chosen. Additionally, we took into account the isotopic effect that deuterium has on retention time by applying a 1 min retention time tolerance for isotope pattern multiplets and allowing spectra with 2 missing channels to be quantified. After identification and quantification, we processed all phosphoproteomic and proteomics results according to very stringent peptide acceptance criteria. These criteria include: (i) a false discovery rate (FDR) of less than 1% at the peptide level utilizing the Percolator-based algorithm,[33] (ii) peptides needed to have a Mascot ion score of at least 20 and (iii) peptide length was restricted between 6 and 45 residues. Subsequently, we defined two classes of phosphopeptides and phosphosites: a phosphopeptide was designated Class I when the PhosphoRS site probability for each phosphorylated residue within the phosphopeptide was at least 75%. Also, a phosphosite was designated Class I when its PhosphoRS site probability was at least 75%. All phosphopeptides and -sites that did not conform to this criterion were designated Class II. For a particular phosphosite, the ratio between the 007-AM and mock stimulated condition was determined by the least phosphorylated Class I peptide-spectrum match (PSM) with the highest intensity.

The MS data associated with this manuscript is available as .msf file on tranche at https://proteomecommons.org using the following hash: cUNvwhH9iDkYOzI3kqEQVS7eO4zRNujVpI0BTgk9spKE-qrwE2hhpGOoK05bdRYuRFYc52NEsurA5SvN+a1rqUVy31AUA-AAAAAAAF5g==. The passphrase is ''HUVEC''. The files can be viewed with the Proteome Discoverer software (version 1.3) or the Thermo MSF Parser (version 1.0.3), which is freely available at http://code.google.com/p/thermo-msf-parser/.

Kinase motif classification and amino acid frequency overrepresentation analyses

To predict which protein kinase phosphorylated the identified phosphorylation site, we used the group-based prediction system (GPS, version 2.1).[34,35] GPS uses well-established rules to classify human protein kinases for prediction by utilizing kinase family hierarchy and protein–protein interaction data. Thereby, it provides an accurate, powerful and high-throughput approach for the prediction of phosphorylation site-specific protein kinases. Predicted kinases were divided into basophilic, proline-directed, acidophilic, tyrosine or other kinase classes.[36] To determine whether a particular kinase class was significantly over- or underrepresented for the predicted kinases for the up- or

downregulated phosphosites, we performed statistical analyses using a two-tailed Fisher's exact test. The number of up- or downregulated phosphosites belonging to a particular kinase class was compared to the number of predicted kinases belonging to that same class in all identified Class I phosphosites.

Amino acid overrepresentation analyses were performed using the freeware program IceLogo (version 1.2),[37] which can be found at http://code.google.com/p/icelogo/. All phosphosites were aligned to the center of a sequence containing 7 amino acids surrounding either side of the phosphosite. The experimental sets for the analyses consisted of the 1.5-fold up- or downregulated aligned phosphorylation sites. The background comprised all aligned Class I phosphorylation sites. The *P*-value for all analyses was set at ≤ 0.05.

STRING network, pathway and GO term enrichment analyses

Protein network analysis was performed using a search tool for the retrieval of interacting genes (STRING, version 9.0),[38,39] which can be found at http://string-db.org/. The input list contained all regulated phosphoproteins and, in addition, the Epac proteins (Epac1, Epac2) and Rap proteins (Rap1A, Rap1B, Rap2A, Rap2B, and Rap2C), as they are regulated by 007-AM in a direct and indirect manner, respectively. To obtain a high quality network in which known interactions were preserved, we set the ''required confidence'' at ''high'' (0.7). For visualization purposes, the obtained STRING network data were imported into the Cytoscape software[40] (version 2.8.3), which can be found at http://www.cytoscape.org/.

The database for annotation, visualization and integrated discovery (DAVID)[41,42] was used for both the pathway and the gene ontology (GO) term enrichment analyses and can be found at http://david.abcc.ncifcrf.gov/. The experimental set contained all phosphoproteins that displayed 1.5-fold up- and downregulated phosphorylation sites after 007-AM stimulation. In addition, the Epac and Rap proteins were included in the experimental set for the reason mentioned above. To minimize experimental bias, the analyses were performed against a background set that consisted of all identified phosphoproteins, which included those that are regulated and not regulated. A pathway or GO term was considered to be significantly overrepresented if its expression analysis systematic explorer (EASE) score, a modified Fisher's exact *P*-value, was ≤ 0.05.

Results

Cell treatment, dimethyl labeling and SCX chromatography

To investigate the downstream effects of Epac-Rap signaling on protein phosphorylation in a confluent monolayer of HUVECs, we employed a quantitative global phosphoproteomic approach. The downstream effects of Rap activation were maximized by replicating experimental conditions that were previously shown to significantly increase the stimulatory window of the Epac-specific cAMP analogue 007-AM on HUVEC barrier function as measured by electric cell–substrate impedance sensing (ECIS).[12] This was achieved by depletion of the Rap exchange factors PDZ-GEF1 and PDZ-GEF2, which decrease the basal barrier function. Indeed, depletion of both PDZ-GEF1 and 2 in a monolayer of HUVECs results in a strong reduction in basal impedance, indicating a decrease in the basal endothelial barrier function (Fig. 1A). Importantly, this drop in basal impedance can be almost fully rescued by 007-AM stimulation, thereby providing an increase in the stimulatory window. The drop in basal barrier function is associated with the zipper-like staining of the junctional marker protein β-catenin (Fig. 1B). Stimulation with 007-AM induced a straightening of the β-catenin staining and gave rise to actin cytoskeletal rearrangements that reduce the amount of transverse actin fibers spanning the cell body and increase the amount of cortical actin bundles colocalizing with the cell–cell contacts, which are also known as junctional actin.[12] To ensure the identification of direct phosphorylation targets and to prevent a large contribution of potential feedback signaling, 15 minutes of 007-AM stimulation was chosen. This is the shortest timeframe in which the barrier function of a HUVEC monolayer increases to its maximum and stable level upon 007-AM stimulation (Fig. 1A).

The experiment was performed in duplicate in the following manner: in the first experiment, designated 'Forward', 2 mg of HUVEC lysate was digested for the mock stimulated control as well as for the 007-AM stimulated condition. Subsequently, the control cells were labeled with light dimethyl labels and the 007-AM stimulated cells were labeled with intermediate dimethyl labels. In the duplicate experiment, designated 'Reverse', 2 mg of HUVEC lysate was digested for each condition as well. However, for the dimethyl labeling procedure the labels were swapped compared to the 'Forward' experiment. Thus, the control cells were labeled with intermediate dimethyl labels and the 007-AM stimulated cells were labeled with light dimethyl labels. Next, the differentially labeled samples were mixed in a 1 : 1 ratio and subjected to low pH SCX separation to fractionate the peptides based on their charge state. Some of the SCX fractions were pooled depending on their estimated phosphopeptide content, reducing the 40 initial fractions to a total of 33 fractions per experiment. Importantly, all 66 SCX fractions were desalted as the phosphate that is present in the SCX solvents interferes with the subsequent phosphopeptide enrichment step. An overview of the experimental workflow covering the above-mentioned steps and subsequent steps described below is depicted in Fig. 2.

Ti^{4+}-IMAC-based phosphopeptide enrichment, MS analysis, phosphorylation site localization and ddDT/CID-MSA LC-MS/MS performance

To achieve an in-depth coverage of the HUVEC phosphoproteome, we employed Ti^{4+}-IMAC-based enrichment as we recently showed this to be one of the most comprehensive ways to target the phosphoproteome.[20] Therefore, each of the 66 SCX fractions was subjected to Ti^{4+}-IMAC enrichment. In addition, we have recently shown that instructing an Orbitrap Velos mass spectrometer to fragment peptides using higher-energy collisional dissociation (HCD), electron transfer dissociation (ETD) or ETD with Orbitrap readout (ETD FT), depending on their precursor charge state, significantly improves the average

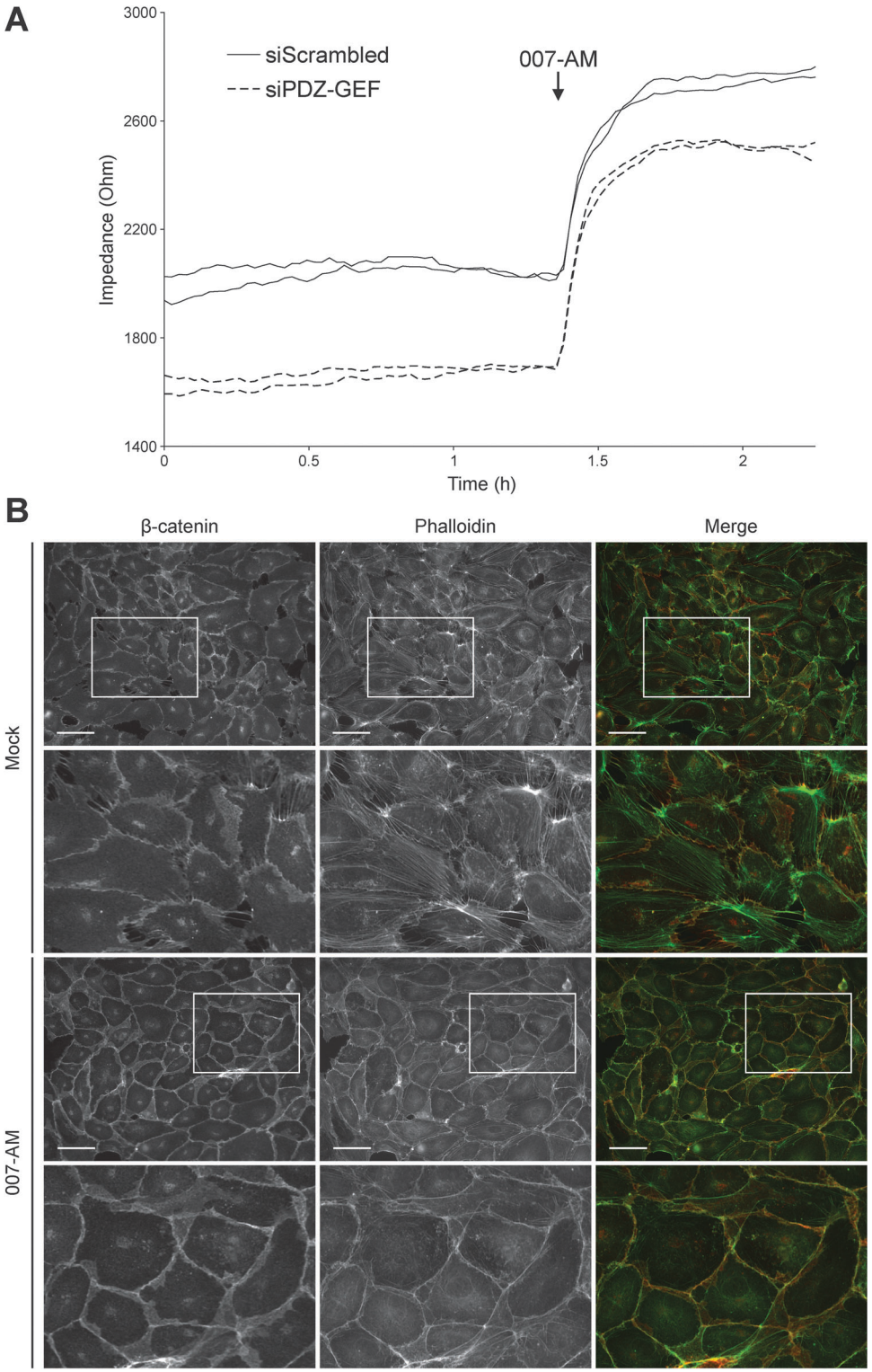

Fig. 1 Rap activation through 007-AM in cells depleted of PDZ-GEF results in restoration of the barrier function, straightening of cell–cell contacts and the formation of junctional actin. (A) Time-lapse electric cell–substrate impedance sensing (ECIS) recording of human umbilical vein endothelial cells (HUVECs) transfected with siScrambled (continuous line) or both siPDZ-GEF1 and siPDZ-GEF2 (siPDZ-GEF) (dashed line). When indicated, 8-pCPT-2′-*O*-Me-cAMP-AM (007-AM) was added to a final concentration of 1 μM. (B) Immunofluorescence staining of HUVECs transfected with both siPDZ-GEF1 and siPDZ-GEF2. Cells were stained for β-catenin (left panels, red in merge), and phalloidin, which stains actin, (middle panels, green in merge). When indicated, 007-AM was added to a final concentration of 1 μM. An enlargement of the cells within the white rectangle is shown below each panel. Scale bar: 50 μm.

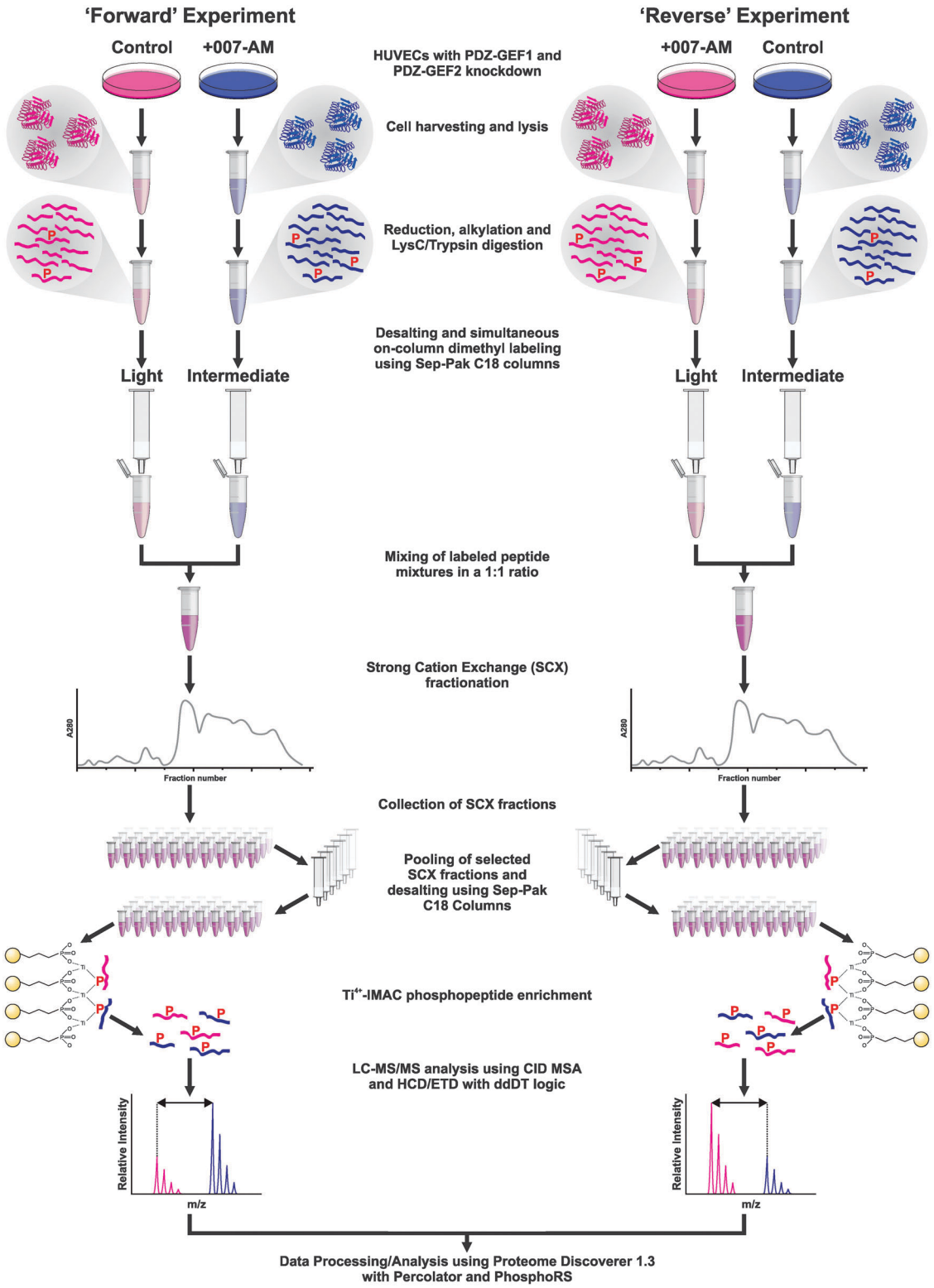

Fig. 2 Overview of the experimental workflow. The phosphoproteome of the 8-pCPT-2′-*O*-Me-cAMP-AM (007-AM) treated human umbilical vein endothelial cells (HUVECs) was probed in duplicate. In the 'Forward' experiment, mock treated HUVECs were labeled with light dimethyl labels and 007-AM stimulated cells with intermediate dimethyl labels. In the 'Reverse' experiment the labels were swapped. Subsequently, samples were mixed in a 1 : 1 ratio and fractionated by low pH strong cation exchange (SCX). Some of the initial SCX fractions were pooled, depending on their estimated phosphopeptide content, and the resulting fractions were desalted and subjected to titanium(IV) immobilized metal affinity chromatography (Ti^{4+}-IMAC) phosphopeptide enrichment. Finally, all fractions were analyzed by liquid chromatography–mass spectrometry/mass spectrometry (LC-MS/MS) using collision-induced dissociation–multistage activation (CID-MSA) or higher-energy collisional dissociation (HCD)/electron transfer dissociation (ETD) using a data-dependent decision tree (ddDT) logic.

Table 1 Number of identified phosphopeptides, phosphosites and phosphoproteins

	Total: Class I & Class II (# of unique hits)			Unambiguous: Class I (# of unique hits)			Unambiguous & quantified: Class I & quantified (# of unique hits)	
	Phospho-peptides	Phospho-sites	Phospho-proteins	Phospho-peptides	Phospho-sites	Phospho-proteins	Phospho-sites	Phospho-proteins
Forward	12 684	10 982	3362	10 929	9 549	3204	8327	2798
Reverse	16 475	14 380	4090	14 144	12 280	3836	10 377	3235
Total	19 859	17 278	4594	16 800	14 617	4298	12 118	3509

Mascot score.[24] Therefore, we used this method, which is defined in a modified ddDT algorithm, to analyze all enriched SCX fractions. In addition, the enriched SCX fractions containing the largest amount of 'neutral phosphopeptides' (fractions 12–15, termed 'main phosphofractions' hereafter) were reanalyzed using a CID-MSA method. Using these methods, we were able to identify a total of 19 859 unique phosphopeptides containing 17 278 unique phosphorylation sites on 4594 phosphoproteins after filtering for a minimum Mascot score of 20 and an FDR of less than 1% using Percolator (Table 1). When considering the separate 'Forward' and 'Reverse' experiments, we identified 12 684 unique phosphopeptides containing 10 982 unique phosphosites on 3362 phosphoproteins in the 'Forward' experiment and 16 475 unique phosphopeptides possessing 14 380 unique phosphosites on 4090 phosphoproteins in the 'Reverse' experiment (Table 1). The overlap of the identified unique phosphopeptides in the 'Forward' and 'Reverse' experiments was between 56 and 73 percent (ESI,† Fig. S1, first panel).

As the exact location of a specific phosphosite within its corresponding phosphopeptide cannot always be unambiguously determined by the database search algorithm, we employed the PhosphoRS algorithm, which is included in the Proteome Discoverer 1.3 software, to determine the localization probability for each phosphosite. This algorithm was generated, validated and optimized based on the fragmentation spectra of a training set of 150 synthetic phosphopeptides with known phosphorylated residues, which were selected as a representative reflection of phosphorylated peptides present in any phosphoproteome.[32] We define an unambiguously localized phosphopeptide, hereafter called a Class I phosphopeptide, as a phosphopeptide that possesses a PhosphoRS site probability of at least 75% for each of its phosphorylation sites. A phosphosite was designated Class I if its own PhosphoRS site probability was at least 75%, independent of the presence of another phosphosite in the same PSM that did not comply to this criterion. In this way, multiply phosphorylated PSMs that possess one or more poorly localized phosphorylated residues were not considered to be Class I phosphopeptides but the phosphorylated residues that are unambiguously localized were considered to be Class I phosphorylation sites. All phosphopeptides and -sites that did not comply with these criteria were designated Class II. Application of these filter criteria gave rise to 16 800 Class I phosphopeptides and 14 617 Class I phosphosites on 4298 phosphoproteins. All identified unique Class I and Class II phosphopeptides and -sites are listed in Tables S1 and S2 (ESI†), respectively. The total amount of unique Class I phosphopeptides identified in each fraction is depicted in Fig. 3A. The identified unique Class I and Class II phosphopeptides and -sites for the separate 'Forward' experiment are listed in Tables S3 and S4 (ESI†), respectively. Those identified in the 'Reverse' experiment are listed in Tables S5 and S6 (ESI†). Fig. S2 (ESI†) shows the total amounts of unique Class I phosphopeptides identified in each fraction for the 'Forward' and 'Reverse' experiments separately.

The unique phosphopeptide with the highest PhosphoRS score was used to determine which fragmentation technique gave rise to the identification of this peptide and in which fraction it was identified. The overlap of the identified unique Class I phosphopeptides and Class I phosphosites between the 'Forward' and 'Reverse' experiments was 58 to 79 percent (ESI,† Fig. S1, second and third panels). For each enriched SCX fraction we examined which fragmentation technique contributed to the highest percentage of the identified unique Class I phosphopeptides. When we only considered the highest scoring unique peptides identified using either HCD or ETD, thereby leaving out those identified using CID-MSA, we observed that ETD clearly contributes to more identifications than HCD for the late SCX fractions. This particularly holds true for fractions 31–40, which contain the 'positive phosphopeptides' (Fig. 3B). In contrast, HCD contributes to more identifications than ETD for the earlier SCX fractions and in particular the main phosphofractions containing the 'neutral phosphopeptides'. When taking all fragmentation techniques into account for the main phosphofractions only, CID-MSA contributes to a substantial part (39%) of the total amount of highest scoring unique phosphopeptides identified in each of these fractions, thereby matching the performance of HCD (42%) (Fig. 3C).

Comparison of this dataset with previously published data for a number of proteins reveals numerous novel phosphorylation sites

To exemplify the scale of this (endothelial) phosphoproteome, a number of proteins were selected and the unique Class I phosphorylation sites identified in this study were compared to those previously published (as curated at http://www.uniprot.org) and mapped onto their domain structure (Fig. 4). Previously published phosphosites not identified in this study are depicted in black, those also identified in this study are depicted in blue and novel phosphosites are depicted in green. For the junctional protein p120 catenin/catenin delta-1 (Uniprot

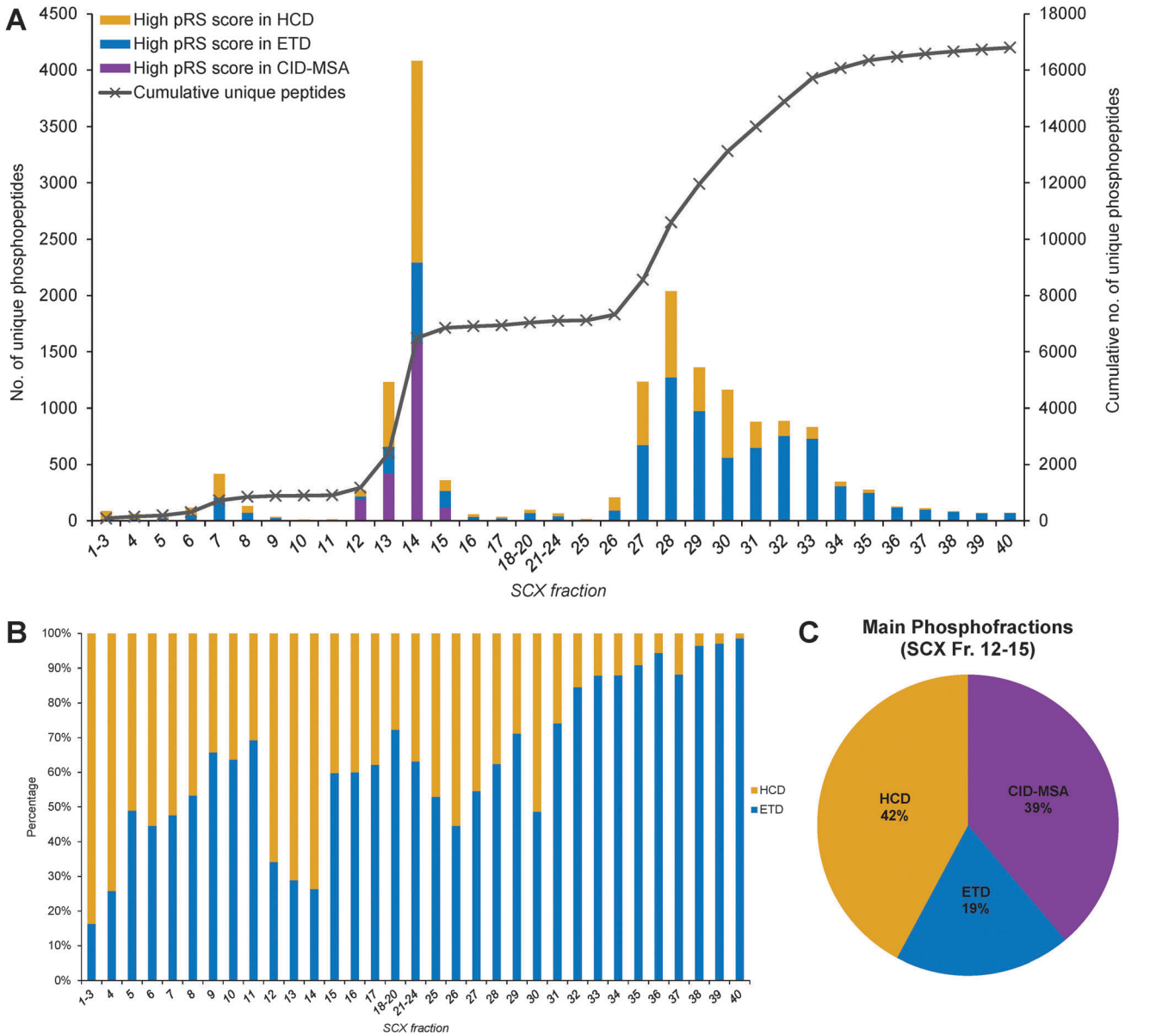

Fig. 3 Analysis of the number of unique Class I phosphopeptides and phosphorylation sites identified per fraction. (A) Bar chart showing the number of unique highest scoring Class I phosphopeptides identified per fraction and the fragmentation methods by which they were identified (higher-energy collisional dissociation (HCD) in yellow, electron transfer dissociation (ETD) in blue, and collision-induced dissociation–multistage activation (CID-MSA) in purple). The cumulative amount of identified unique Class I phosphopeptides per fraction is plotted as a grey line, using the *y*-axis on the right-hand side, in which a cross marks each fraction. (B) Bar chart depicting to which percentage of the identified unique highest scoring Class I phosphopeptides either HCD (yellow) or ETD (blue) contributed for each fraction. Unique phosphopeptides identified by CID-MSA (only used for fractions 12–15) were not taken into account. (C) Pie chart displaying to which percentage of the identified unique highest scoring Class I phosphopeptides HCD (yellow), ETD (blue), or CID-MSA (purple) contributed for the main phosphofractions.

accession # O60716), we identified 37 unique phosphosites of which 11 have been previously reported (Fig. 4, top). Our study identifies 26 novel sites, which almost doubles the number of reported p120 catenin phosphosites (from 28 to 54). For the Rap effector afadin/AF6 (Uniprot accession # P55196) we identified 21 unique phosphorylation sites (Fig. 4, middle), of which 9 have been reported before and the other 12 are novel. This leads to a total number of 27 phosphosites that have currently been identified for AF6. Finally, for the endothelial-specific protein endothelial nitric oxide synthase (eNOS/NOS3) (Uniprot accession # P29474) only 2 sites have previously been reported (Fig. 4, bottom). This endothelial phosphoproteome contains 13 phosphorylation sites on eNOS, of which 1 has previously been published, thus giving rise to 12 novel sites, making a total of 14 currently identified phosphosites.

Taken together, these examples demonstrate that our dataset significantly contributes to the identification of protein phosphorylation sites by revealing many novel phosphosites. Moreover, our dataset may contain particularly valuable information on phosphorylation sites for endothelial-specific proteins.

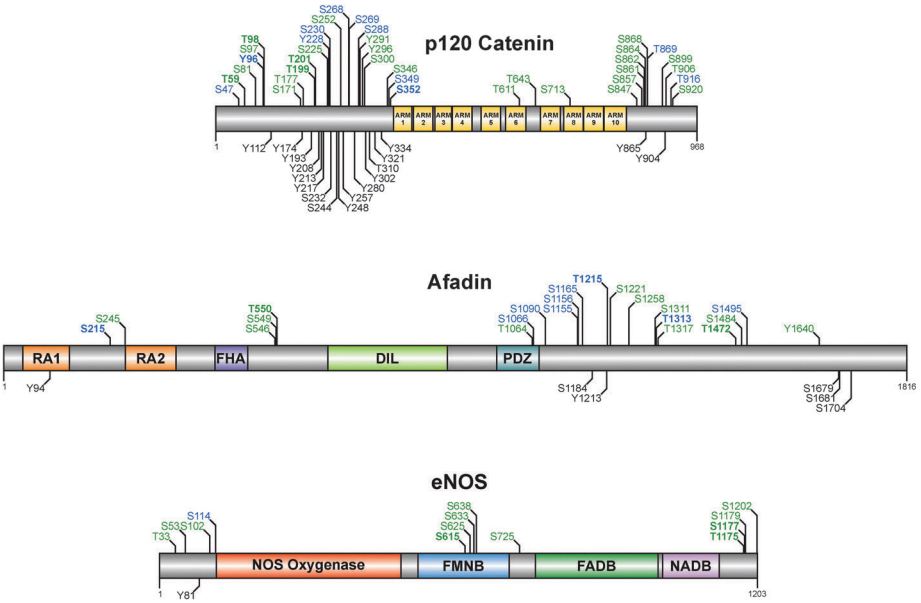

Fig. 4 This phosphoproteome dataset significantly contributes to the identification of novel (endothelial-specific) phosphorylation sites. Domain structures of the junctional protein p120 catenin/catenin delta-1 (top), the Rap effector AF6/afadin (middle) and the endothelial-specific protein endothelial nitric oxide synthase (eNOS/NOS3) (bottom). Previously published phosphosites that were not identified in this study are depicted in black, those that are also identified in this study are depicted in blue and novel phosphosites are depicted in green. Phosphosites that were found to be regulated (see Fig. 5 and associated text) are depicted in boldface characters. ARM, armadillo repeat; RA, Ras-association domain; FHA, forkhead-associated domain; DIL, dilute domain; PDZ, PSD-95/DlgA/ZO-1; NOS oxygenase, nitric oxide synthase oxygenase; FMNB, FMN binding domain; FADB, FAD binding domain; NADB, NAD binding domain.

Phosphorylation site quantification results in 220 phosphosites that are at least 1.5-fold regulated upon 007-AM stimulation

To obtain information concerning the regulation of phosphosites upon 007-AM stimulation, it is crucial to determine which of the Class I phosphopeptides are quantified by the Proteome Discoverer software so that the relative ratio between the 007-AM and mock stimulated conditions can be calculated for a particular phosphosite. These phosphosite ratios were determined by the least phosphorylated version of the corresponding Class I PSM with the highest intensity. Taking this into account we identified a total of 12 118 quantified unique Class I phosphosites on 3509 phosphoproteins (Table 1). The overlap of the identified unique quantified unique Class I phosphosites between the 'Forward' and 'Reverse' experiments was 63 to 79 percent, resulting in 6586 sites that could be co-quantified (ESI,† Fig. S1, fourth panel; ESI,† Table S7). When taking the 'Forward' and 'Reverse' experiments into account separately, we identified 8327 and 10 377 quantified unique Class I phosphorylation sites on 2798 and 3235 phosphoproteins, respectively (Table 1, ESI,† Tables S8 and S9).

We decided to designate a particular phosphosite as being regulated by 007-AM when it was identified in a Class I phosphopeptide, its ratio $\geq$1.5-fold (or its $\log_2$ value of 0.58) changed compared to the unstimulated control and most importantly when these peptides were found to be regulated in the same direction in both experiments. The chosen cutoff of 0.58 is well outside the one time standard deviation value of 0.42 for the given dataset but still allows a good insight into the 007-AM regulated phosphorylation sites. The performance of the stable isotope dimethyl labeling in terms of technical variation has been reported.[43] All co-quantified unique Class I phosphosites and their corresponding $\log_2$ ratios are plotted in Fig. 5. Those that are 1.5-fold up- or downregulated in both experiments are depicted in blue and yellow, respectively. We identified 94 upregulated unique phosphosites in 79 phosphoproteins and 126 downregulated unique phosphosites in 100 phosphoproteins (ESI,† Table S10). In total, 166 proteins were differentially phosphorylated upon 007-AM stimulation. Several phosphoproteins possess multiple regulated phosphosites, of which the most apparent are p120 catenin/catenin delta-1 (CTNND1) and AF6 (MLLT4/afadin) that harbor 6 and 5 downregulated unique phosphorylation sites, respectively. Interestingly, overall we identify more downregulated than upregulated phosphosites: 126 *versus* 94, respectively. A total of 13 phosphoproteins simultaneously contain up- and downregulated phosphosites. Importantly, we do not observe any significantly up- or downregulated proteins due to the 007-treatment (ESI,† Fig. S3).

Kinase motif classification and amino acid frequency overrepresentation analyses reveal that upregulated phosphosites are mainly targets of basophilic kinases whereas downregulated sites mainly belong to proline-directed kinases

In order to gain insight into which kinases are responsible for phosphorylation events downstream of 007-AM stimulation, we employed the group-based prediction system (GPS) kinase prediction software.[34,35] We were able to predict a potential kinase group, family and/or subfamily for 30 out of 94 upregulated phosphosites (32%) and 33 out of 126 downregulated phosphosites (26%) (ESI,† Table S3). For the background set,

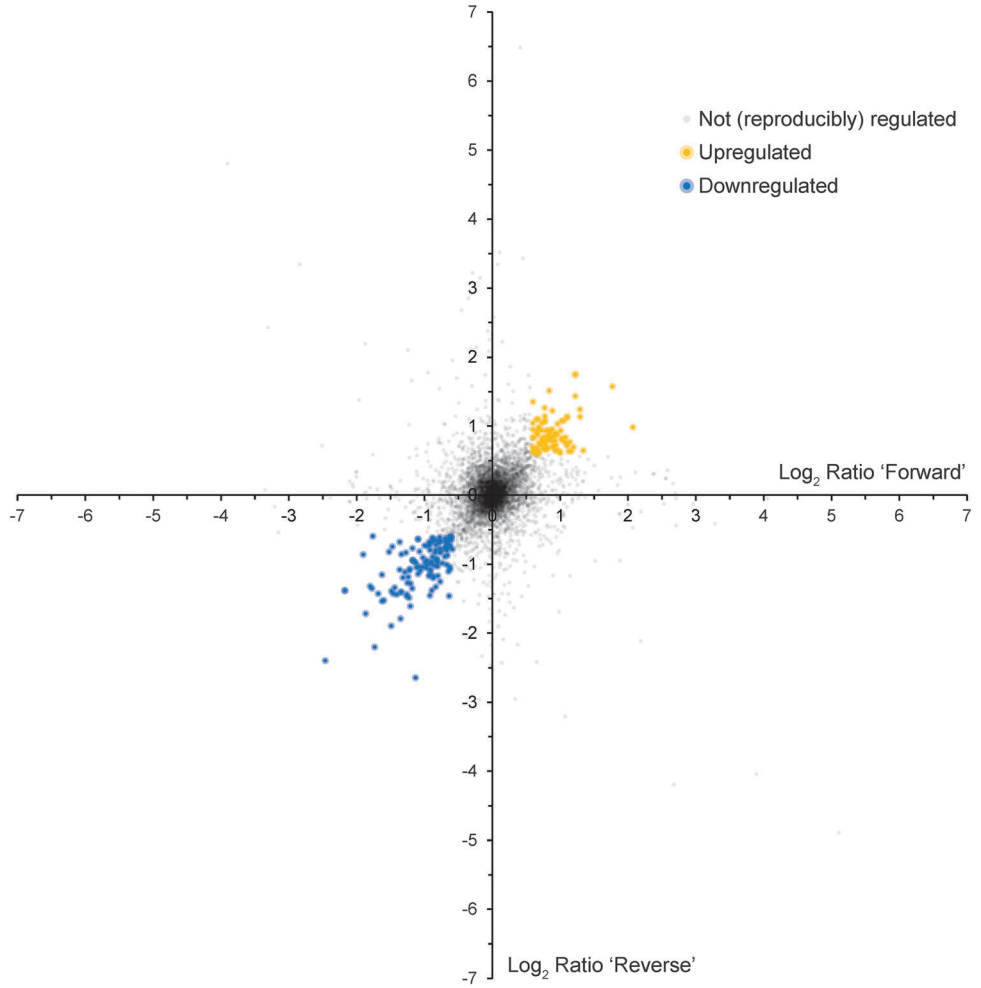

Fig. 5 Overview of the ratios of all co-quantified unique phosphorylation sites. Scatter plot depicting the $\log_2$ ratios of all identified quantified unique Class I phosphosites that were quantified in both the 'Forward' and the 'Reverse' experiment (Mascot score ≥ 20, false discovery rate (FDR) $< 1\%$, PhosphoRS site probability $\geq 75\%$). Phosphosites that are ≥ 1.5-fold downregulated upon 8-pCPT-2′-*O*-Me-cAMP-AM (007-AM) treatment in both experiments are depicted in blue ($n = 126$) and those that are ≥ 1.5-fold upregulated in yellow ($n = 94$). Phosphosites that showed no regulation or no reproducible regulation ($n = 6366$) are shown as semi-transparent black dots.

containing all Class I phosphosites, we were able to predict a kinase for 3618 phosphosites (25%). We divided these kinases into basophilic, proline-directed, acidophilic, tyrosine or other kinase classes,[36] and when we examined the kinase classes associated with upregulated phosphosites downstream of 007-AM treatment, we observed that basophilic kinases (70%) are significantly overrepresented when compared to the background set (28%) (Fig. 6A). In contrast, proline-directed kinases (3%) are significantly underrepresented when the pool of 007-AM upregulated phosphosites is compared to the background set (35%). Interestingly, when we look at the downregulated phosphosites, we observe that target sites of proline-directed kinases are significantly more often dephosphorylated (55%). In contrast, those of basophilic kinases (9%) are significantly less frequently dephosphorylated. Moreover, 72% of the downregulated proline-directed kinase sites are predicted to be target sites of cyclin-dependent kinases (CDKs). This remarkable difference in kinase classes regulating the upregulated and downregulated sites is quite striking.

To further explore these observations and to see whether there is a general consensus motif present surrounding either the up- or downregulated phosphorylation sites, we used the freeware program IceLogo to reveal any statistically significant over- or underrepresentation in the frequency with which a particular amino acid is present at a certain position.[37] Importantly, IceLogo can plot these frequency differences using an experimental set and a background set as a reference, thereby minimizing the influence of the used experimental protocol and also allowing the addition of statistical significance to underrepresented amino acids. Overrepresentation of a particular amino acid yields a positive value, whereas underrepresentation a negative value, and this is plotted as a measure of the height of a letter in an amino acid stack. The background consisted of all identified phosphorylation sites aligned to the center of a sequence containing 7 amino acids surrounding either side of the phosphosite. The experimental sets were either the aligned sequences of the upregulated phosphosites or those of the downregulated ones. P – *n* indicates the amino acid *n* residues

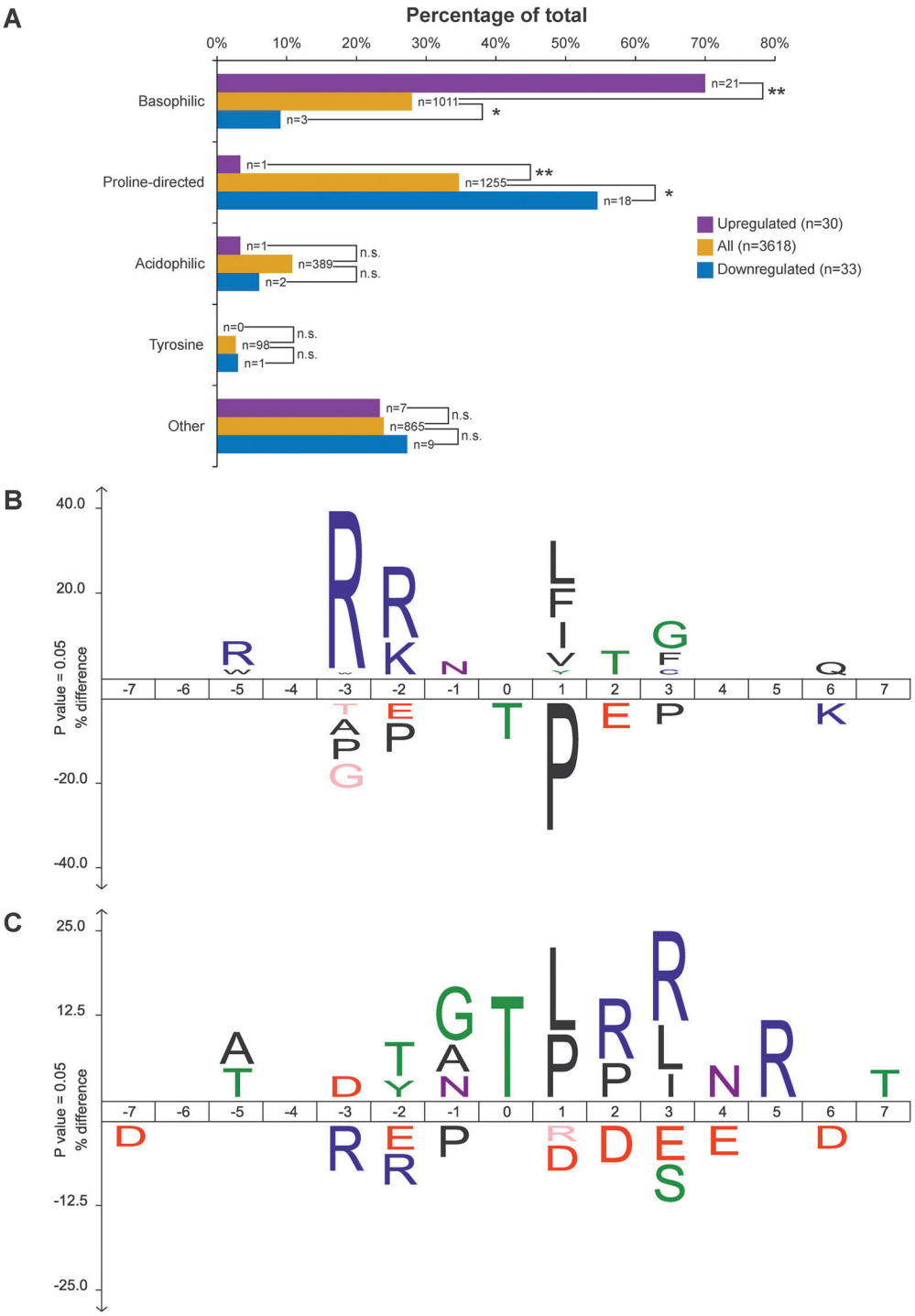

Fig. 6 Basophilic kinases mainly fulfill upregulation, whereas downregulated phosphosites are predominantly target sites of proline-directed kinases. (A) Bar chart depicting the relative distribution of the kinases classes assigned to the upregulated (purple bars) or downregulated (blue bars) phosphorylation sites. For comparison, the percentage by which a particular kinase class was present in the set of all identified Class I phosphosites is depicted (yellow bars). Statistical analysis was performed using a two-tailed Fisher's exact test. Asterisks indicate the *P*-value of the respective sample with the associated control sample. $*P < 0.02$; $**P < 0.0001$; n.s., not significant. (B) IceLogo for all phosphosites that are upregulated upon 007-AM treatment displaying significantly over- and underrepresented amino acid residues at particular positions surrounding the phosphorylation site (position 0), using all identified phosphorylation sites as the background (*P*-value ≤ 0.05). (C) IceLogo for all phosphosites that are downregulated upon 8-pCPT-2′-*O*-Me-cAMP-AM (007-AM) treatment, displaying significantly over- and underrepresented amino acid residues at particular positions surrounding the phosphorylation site (position 0), using all identified phosphorylation sites as the background (*P*-value ≤ 0.05).

located N-terminally to the phosphosite and P + *n* indicates the amino acid *n* residues located C-terminally to the phosphosite.

We first determined whether there are any significantly increased amino acid frequencies present in the sequences

surrounding the upregulated phosphosites compared to the background set. The most apparent are those of basic residues at positions P-5, P-3 and P-2, where arginine and lysine residues are more frequently observed (Fig. 6B). This is a hallmark of target sites for basophilic kinases such as protein kinase A (PKA), and protein kinase B (PKB/Akt).[36,44] At P + 1 the hydrophobic amino acids leucine, phenylalanine, isoleucine and valine residues were found more frequently. Interestingly, we were able to discern that a proline residue was found less frequently at position P + 1. Furthermore, threonine residues seemed to be less frequently phosphorylated when compared to the background set.

In the set of downregulated phosphorylation sites, we observe that threonine residues are more frequently dephosphorylated and that at position P + 1 leucine and proline residues are found with a higher frequency compared to the background set (Fig. 6C). This confirms the results from our kinase motif analyses, indicating that the target sites of proline-directed kinases are more frequently dephosphorylated. Interestingly, the increased frequency of leucine at position P + 1 might suggest the involvement of a novel class of kinases that recognize a leucine residue at this position. In addition, the frequency with which the basic residue arginine occurs C-terminally to the phosphorylation site is increased, while the acidic residues glutamic acid and aspartic acid are less frequently occurring on this side. Moreover, the occurrence of arginine residues at positions P-2 and P-3 is less frequent compared to the background set, indicating a decreased dephosphorylation rate of target sites of basophilic kinases.

Taken together, the kinase prediction and amino acid frequency overrepresentation data both indicate that basophilic kinases are mainly responsible for phosphorylation events downstream of 007-AM stimulation and that sites that are downregulated are target sites of proline-directed kinases.

STRING network analysis on 007-AM regulated phosphoproteins reveals protein network modules involved in actin-cytoskeleton remodeling, cell junction organization and cell–substratum adhesion, and is confirmed by pathway and GO term analyses

To examine whether the 007-AM regulated phosphoproteins are part of known protein networks, we analyzed these proteins using a search tool for the retrieval of interacting genes (STRING)[38,39] and visualized the network data using the Cytoscape software. STRING is a meta-database constructed on the basis of both physical and functional interactions and outputs a graphical representation of the identified protein networks that are present within a queried list of proteins of interest. The input list we used included all regulated phosphoproteins and also Rap1A, Rap1B, Rap2A, Rap2B, Rap2C, Epac1 and Epac2, as 007-AM regulates these proteins either directly or indirectly. Several modules of interacting proteins become apparent from the STRING output (Fig. 7). We can distinguish at least 4 predominant modules of proteins: the first contains the Rap-related proteins, including the Rap and Epac proteins but also the known Rap effectors AF6 (MLLT4/afadin), TRAF2 and NCK-interacting protein kinase (TNIK) and NCK-interacting kinase (MAP4K4/NIK) and the Rap-interacting protein Ras-interacting protein 1 (RASIP1). The second module contains proteins involved in Rho GTPase signaling and actin cytoskeleton dynamics, including Rho-associated protein kinase 1 (ROCK1), Rho-associated protein kinase 2 (ROCK2), LIM domain kinase 2 (LIMK2) and protein phosphatase 1 regulatory subunit 14B (PPP1R14B). The third module contains proteins that are involved in cell junction organization and their attachment to the actin cytoskeleton. These include tight junction protein 1/ZO-1 (TJP1/ZO-1), tight junction protein 2/ZO-2 (TJP2/ZO-2), alpha catenin/catenin alpha-1 (CTNNA1), p120 catenin/catenin delta-1 (CTNND1), claudin 5 (CLDN5), LIM domain only protein 7 (LMO7), armadillo repeat protein deleted in velo-cardio-facial syndrome (ARVCF) and the proteins vinculin (VCL), zyxin (ZYX) and vasodilator-stimulated phosphoprotein (VASP), which have also been linked to focal adhesions, and connect to the last module of integrin signaling proteins, including integrin beta-4 (ITGB4), integrin beta-5 (ITGB5) and talin 1 (TLN1). The rationale behind constituting these specific modules, including the relevant references, is described in the discussion section. Thus, the STRING network analysis confirms a number of known Rap effectors and Rap-interacting proteins and additionally shows modules of proteins that are involved in actin-cytoskeleton remodeling, cell junction organization and cell–substratum adhesion.

To get additional biologically relevant information on the phosphoproteins that displayed a regulated phosphorylation status upon 007-AM treatment, we determined whether specific biological pathways or gene ontology (GO) terms, associated with these phosphoproteins, were overrepresented. To achieve this, we made use of the database for annotation, visualization and integrated discovery (DAVID), which is an online meta-tool that offers a wide array of overrepresentation analyses.[41,42] In order to minimize any bias as a result of the utilized experimental procedure, we used the entire list of identified phosphoproteins, containing both the regulated and the unregulated ones, as the background. In this way, we are able to identify 9 biological pathways that are significantly overrepresented in the list of 007-AM regulated phosphoproteins (ESI,† Fig. S4A, and Table S11). When we look at the GO term enrichment of proteins with 007-AM regulated phosphorylations, we observe that 17, 29 and 13 GO terms from the biological process (BP), cellular compartment (CC) and molecular function (MF) domains are significantly enriched, respectively (ESI,† Fig. S4B–D, and Table S11). Taken together, the biological pathway and GO term enrichment analyses confirm the results of the STRING network analysis and reveal that the majority of the phosphoproteins that are regulated upon 007-AM treatment are involved in cell–cell adhesion, cell–substratum adhesion, and cell motility. Some of these processes are regulated through Rho GTPase signaling, actin and microtubule cytoskeletal rearrangements, cell–cell junction formation, and the formation of cellular projections. These processes occur predominantly at cell junctions, the actin and microtubule cytoskeleton, the plasma membrane, and cellular projections and require physical interaction of some of these proteins with the actin cytoskeleton or its substructures.

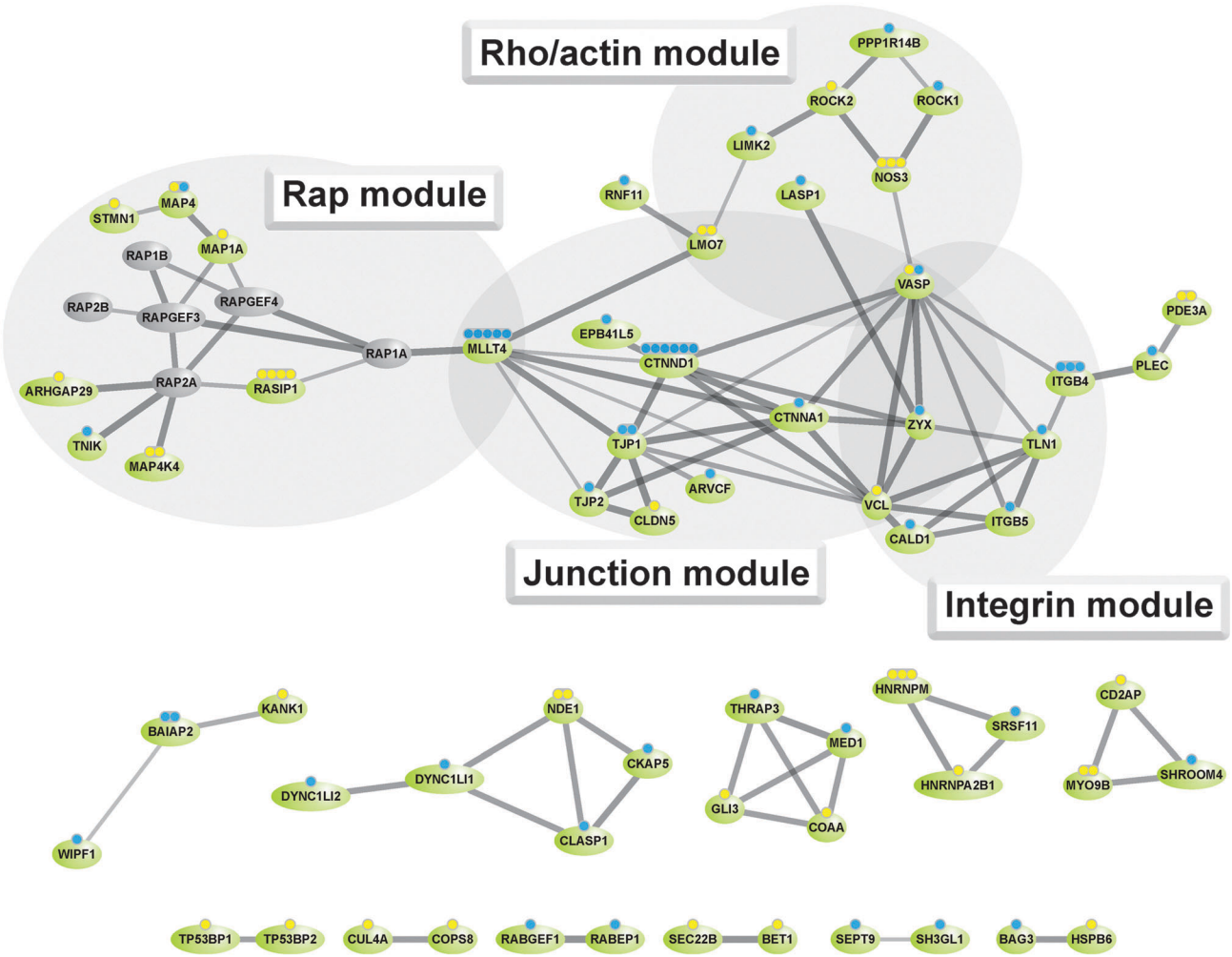

Fig. 7 STRING protein network analysis reveals several modules that display regulated phosphorylation levels upon 007-AM stimulation. 8-pCPT-2′-*O*-Me-cAMP-AM (007-AM) regulated proteins are depicted as green ovals and the number of regulated phosphorylation sites, including the direction of their regulation (upregulated in yellow, downregulated in blue), are indicated for each protein. Groups of proteins that function in related processes are confined to modules that are indicated with grey semi-transparent ovals. The Epac and Rap proteins that were added to the input list are depicted in grey.

Lastly, regulation of Rho GTPases through RhoGEFs and regulation of protein phosphorylation by inhibiting protein phosphatases may be relevant for these processes to take place.

Discussion

Many cellular pathways rely on protein phosphorylation for successful conveyance of their signals. To get an insight into signaling events downstream of Rap signaling in primary endothelial cells, we aimed to identify phosphorylation events that occur upon 007-AM treatment in HUVECs. We identify 19 859 unique phosphopeptides containing 17 278 unique phosphorylation sites on 4594 phosphoproteins. To achieve this in-depth coverage of the HUVEC phosphoproteome, we utilized several state-of-the-art phosphoproteomics techniques including low pH SCX, Ti^{4+}-IMAC, and ddDT- and CID-MSA-LC-MS/MS. We were able to identify 220 unique unambiguous phosphosites on 166 phosphoproteins that are regulated at least 1.5-fold in both experiments, which represents ~1% of the detected phosphoproteome.

CID-MSA, ETD and HCD have complementary contributions to phosphopeptide identifications

More than half of all unique phosphopeptides are identified in the late SCX fractions, which contain the bulk of the tryptic peptide population, and this is in accordance with our previous observations using Ti^{4+}-IMAC.[20] We also observe that HCD contributes to the largest part of the identified unique phosphopeptides in the early SCX fractions; however, ETD does so for the late SCX fractions. This is in line with our previous observations and those made by others and confirm the benefit of combining these two fragmentation techniques.[20,24,45–48] Although the advantage of CID-MSA has been debated,[49,50] it does give a large contribution (39%) to the highest scoring identified unique phosphopeptides in the main phosphofractions in our experimental setup, thereby performing on par with HCD (42%). Possibly, the high phosphopeptide content of

the main phosphofractions and the increased sequencing speed of the LTQ Velos allow the CID-MSA method to be more beneficial.

Upregulated phosphorylation sites are governed by a different kinase class than downregulated ones

According to our kinase motif classification and amino acid overrepresentation analyses, the upregulation of phosphosites is mainly due to the action of basophilic kinases, whereas downregulation occurs predominantly on target sites of proline-directed kinases. This suggests that upon Rap activation a certain class of kinases is activated while another class is inactivated, indicating that multiple signaling pathways are affected. The same type of kinase class switch was observed in a study that employed quantitative phosphoproteomics to investigate vasopressin V2-receptor-dependent signaling[51] and suggests that switching between different classes of kinases may be a more general mechanism in signal transduction.

Interestingly, 72% of the downregulated proline-directed kinases belong to the CDK family, which are master regulators of the cell cycle. Epac itself or together with its target Rap has been implicated in the control of cell proliferation, and another major cAMP target, protein kinase A (PKA), was shown to act synergistically with these proteins in this process in several cases.[52–57] Our observation underlines the link between Epac, Rap, PKA and the cell cycle. However, further investigations are needed to determine whether their effects in HUVECs are proliferative or anti-proliferative and Rap- or PKA-dependent.

Functional data analyses confirm several established Rap-regulated cellular processes and reveal possible downstream targets

Using STRING we were able to discern four major network modules containing several known Rap effectors and their interacting proteins (Rap module) and, moreover, proteins that are directly implicated in Rho GTPase controlled actin-cytoskeleton remodeling (Rho/actin module), cell junction organization (junction module) and cell–extracellular matrix adhesion (integrin module).

The Rap module containing the Rap effectors AF6, NIK and TNIK is directly linked to the junction module and the Rho/actin module. The junction module contains both tight junction components, ZO-1, ZO-2 and claudin 5, and adherens junction proteins, alpha catenin, p120 catenin and ARVCF. In the literature, the link between Rap1 and adherens junctions has been well established. Activation of Rap1 *via* the Epac proteins has been reported to tighten the adherens junctions,[8–11] whereas the depletion of Rap1A inhibits junction maturation.[58] Downstream, the Rap effector AF6 has been reported to interact with p120 catenin, thereby stabilizing the cadherin–p120 catenin complex.[14] Since we find several 007-regulated phosphorylation sites in AF6, this may indicate possible feedback regulation in the Rap signaling pathway. Another Rap effector that has been linked directly to junction stabilization is KRIT1. Together with its interacting protein cerebral cavernous malformations 2 (CCM2), KRIT1 has been proposed to regulate endothelial barrier function *via* its inhibitory effect on RhoA and cell contractility.[15,16] Although we did not identify KRIT1 or CCM2 in our 007 phosphoproteome, STRING analysis clearly discerns a Rho/actin module, containing the downstream kinases, ROCK and LIMK2, and the myosin phosphatase inhibitor PPP1R14B. This, together with reports that the RhoGAPs ArfGAP, RhoGAP, ankyrin repeat and PH domains 3 (ARAP3) and Rho GTPase-activating protein 20 (ARHGAP20/RA-RhoGAP) are direct Rap effectors, underlines the significance of the Rho signaling pathway downstream of Rap.[59,60]

The junction module additionally contains several actin associated proteins, including VASP, zyxin and vinculin, which localize at focal adhesions.[61–63] They thereby link the junctional module to the module of integrin (-interacting) proteins, which includes talin 1, integrin beta-4 and integrin beta-5 (reviewed in ref. 64). In the literature, the Rap effector Rap1-GTP-interacting adapter molecule (RIAM) has been established as a direct link between Rap and cell–extracellular matrix (ECM) adhesion, as overexpression of RIAM induces integrin activation and cell adhesion, and the depletion of RIAM abrogates Rap1 induced adhesion.[65,66] As we do not identify any 007-regulated phosphoproteins that more directly link Rap with the structural components involved in cell–ECM adhesion, such as focal adhesions and integrins, this may well indicate that phosphorylation is not involved in the initial phase of Rap-mediated cell–substrate adhesion. In addition, from our pathway and GO term analyses, we can observe that the biological processes that are affected upon Rap activation include cell–cell adhesion, cell–substratum adhesion, and (Rho GTPase-regulated) actin-cytoskeleton rearrangements, which is in line with the results from the STRING network analysis. These processes may further contribute to Rap regulated changes in cell motility and protrusional activity.

In addition, a significant number of proteins could not be directly grouped into specific modules. These may include proteins that could not be linked to the above-mentioned modules due to the absence of connecting proteins either in the STRING database or our dataset. Alternatively, these proteins may be part of a separate, currently unknown functional module, thereby linking Epac or Rap signaling to other thus-far unrelated cellular processes.

The majority of the detectable phosphorylation events occur during later stages of Rap signaling

The absolute regulation of phosphosites upon Rap activation seems rather limited, affecting only ~1% of the detected phosphoproteome. The limited regulation at the phosphorylation level is supported by the low number of kinases/phosphatases that have been reported to function as direct Rap effectors. For Rap2A only the kinases NIK, TNIK and misshapen-like kinase 1 (MINK) have been described,[67–69] and for Rap1 the Raf kinases have been reported as effector proteins.[70] However, the latter finding was challenged by another study that could not confirm this direct link.[71] Thus, initiating phosphorylation events directly downstream of Rap signaling might occur at a low frequency.

The small response at the phosphoproteome level detected here is quite different from global quantitative phosphoproteomics studies that use cellular stimuli to directly regulate a particular kinase[72–75] or those studying cellular processes known to be greatly dependent on phosphorylation.[18,76] Much greater effects on phosphorylation throughout the entire signaling cascade are also observed, as expected. In the Rap signaling pathway, we observe that the majority of phosphorylation events occur much further downstream in structural components of the cell such as adherens junction proteins or actin cytoskeleton-associated proteins.

Conversely, the intermediate phosphorylation events that connect the direct Rap effectors to the structural components of the cell most likely occur in a small and specifically localized subset of proteins. This spatial control of Rap activity is one of the striking features of Rap signaling and is underlined by an abundance of studies describing this particular trait (reviewed in ref. 4). Phosphorylation changes downstream of Rap are therefore most likely modest and difficult to reveal using a global approach: a relatively small change in the global phosphorylation status of a pool of a particular protein may be enough to initiate a certain cellular process if the phosphorylated proteins accumulate at a specific subcellular location. However, as these types of phosphorylations may occur on a small subset of a low abundant pool of proteins, the relatively low stoichiometry makes the corresponding phosphopeptides hard to identify. Therefore, this study may provide only a glimpse of what occurs downstream of Rap activation and mainly includes proteins that act further downstream of Rap. To reveal additional intermediate phosphorylation events, more targeted approaches may be required.

Conclusions

We report the first global phosphoproteome of HUVECs and identify close to 20 000 unique phosphopeptides, making this study one of the most comprehensive datasets to date. Moreover, we report the first quantitative global phosphoproteome after activation of Epac-Rap signaling and identify 220 regulated phosphosites. Our dataset confirms several cellular processes previously linked to Rap, including the maturation and tightening of cell–cell junctions, cell–substratum adhesion and the regulation of cellular tension by the Rho/Rock pathway. Moreover, we now reveal some of proteins that are involved downstream of Rap signaling, including their regulatory phosphorylation sites. Furthermore, we identify additional 007-AM regulated phosphorylation sites in proteins that are not directly linked to these processes. These may constitute novel links between Rap signaling and other currently unrelated cellular processes. Taken together, our dataset reveals several potentially relevant phosphorylation sites and their corresponding proteins, which can serve as a source of information for future studies on Rap signaling.

Acknowledgements

This work was in part supported by the Netherlands Proteomics Centre, embedded in the Netherlands Genomics Initiative, and the Centre for Biomedical Genetics; the Netherlands Organization for Scientific Research (NWO) with a VIDI grant (700.10.429).

References

1 E. Dejana, *Nat. Rev. Mol. Cell Biol.*, 2004, **5**, 261–270.
2 E. Dejana, E. Tournier-Lasserve and B. M. Weinstein, *Dev. Cell*, 2009, **16**, 209–221.
3 J. L. Bos, H. Rehmann and A. Wittinghofer, *Cell*, 2007, **129**, 865–877.
4 M. Gloerich and J. L. Bos, *Trends Cell Biol.*, 2011, **21**, 615–623.
5 J. de Rooij, F. J. Zwartkruis, M. H. Verheijen, R. H. Cool, S. M. Nijman, A. Wittinghofer and J. L. Bos, *Nature*, 1998, **396**, 474–477.
6 H. Kawasaki, G. M. Springett, N. Mochizuki, S. Toki, M. Nakaya, M. Matsuda, D. E. Housman and A. M. Graybiel, *Science*, 1998, **282**, 2275–2279.
7 J. M. Enserink, A. E. Christensen, J. de Rooij, M. van Triest, F. Schwede, H. G. Genieser, S. O. Doskeland, J. L. Blank and J. L. Bos, *Nat. Cell Biol.*, 2002, **4**, 901–906.
8 M. R. Kooistra, M. Corada, E. Dejana and J. L. Bos, *FEBS Lett.*, 2005, **579**, 4966–4972.
9 E. S. Wittchen, R. A. Worthylake, P. Kelly, P. J. Casey, L. A. Quilliam and K. Burridge, *J. Biol. Chem.*, 2005, **280**, 11675–11682.
10 S. Fukuhara, A. Sakurai, H. Sano, A. Yamagishi, S. Somekawa, N. Takakura, Y. Saito, K. Kangawa and N. Mochizuki, *Mol. Cell Biol.*, 2005, **25**, 136–146.
11 X. Cullere, S. K. Shaw, L. Andersson, J. Hirahashi, F. W. Luscinskas and T. N. Mayadas, *Blood*, 2005, **105**, 1950–1955.
12 W. J. Pannekoek, J. J. van Dijk, O. Y. Chan, S. Huveneers, J. R. Linnemann, E. Spanjaard, P. M. Brouwer, A. J. van der Meer, F. J. Zwartkruis, H. Rehmann, J. de Rooij and J. L. Bos, *Cell. Signalling*, 2011, **23**, 2056–2064.
13 W. J. Pannekoek, M. R. Kooistra, F. J. Zwartkruis and J. L. Bos, *Biochim. Biophys. Acta*, 2009, **1788**, 790–796.
14 T. Hoshino, T. Sakisaka, T. Baba, T. Yamada, T. Kimura and Y. Takai, *J. Biol. Chem.*, 2005, **280**, 24095–24103.
15 A. Glading, J. Han, R. A. Stockton and M. H. Ginsberg, *J. Cell Biol.*, 2007, **179**, 247–254.
16 R. A. Stockton, R. Shenkar, I. A. Awad and M. H. Ginsberg, *J. Exp. Med.*, 2010, **207**, 881–896.
17 W. T. Arthur, L. A. Quilliam and J. A. Cooper, *J. Cell Biol.*, 2004, **167**, 111–122.
18 J. V. Olsen, M. Vermeulen, A. Santamaria, C. Kumar, M. L. Miller, L. J. Jensen, F. Gnad, J. Cox, T. S. Jensen, E. A. Nigg, S. Brunak and M. Mann, *Sci. Signaling*, 2010, **3**, ra3.
19 T. Pawson and J. D. Scott, *Trends Biochem. Sci.*, 2005, **30**, 286–290.
20 H. Zhou, T. Y. Low, M. L. Hennrich, H. van der Toorn, T. Schwend, H. Zou, S. Mohammed and A. J. Heck, *Mol. Cell. Proteomics*, 2011, **10**, M110.006452.
21 M. J. Vliem, B. Ponsioen, F. Schwede, W. J. Pannekoek, J. Riedl, M. R. Kooistra, K. Jalink, H. G. Genieser, J. L. Bos and H. Rehmann, *ChemBioChem*, 2008, **9**, 2052–2054.

22 S. A. Beausoleil, M. Jedrychowski, D. Schwartz, J. E. Elias, J. Villen, J. Li, M. A. Cohn, L. C. Cantley and S. P. Gygi, *Proc. Natl. Acad. Sci. U. S. A.*, 2004, **101**, 12130–12135.
23 S. Mohammed and A. HeckJr, *Curr. Opin. Biotechnol.*, 2011, **22**, 9–16.
24 C. K. Frese, A. F. Altelaar, M. L. Hennrich, D. Nolting, M. Zeller, J. Griep-Raming, A. J. Heck and S. Mohammed, *J. Proteome Res.*, 2011, **10**, 2377–2388.
25 M. J. Schroeder, J. Shabanowitz, J. C. Schwartz, D. F. Hunt and J. J. Coon, *Anal. Chem.*, 2004, **76**, 3590–3598.
26 C. Tiruppathi, A. B. Malik, P. J. Del Vecchio, C. R. Keese and I. Giaever, *Proc. Natl. Acad. Sci. U. S. A.*, 1992, **89**, 7919–7923.
27 P. J. Boersema, R. Raijmakers, S. Lemeer, S. Mohammed and A. J. Heck, *Nat. Protoc.*, 2009, **4**, 484–494.
28 H. Zhou, M. Ye, J. Dong, G. Han, X. Jiang, R. Wu and H. Zou, *J. Proteome Res.*, 2008, **7**, 3957–3967.
29 R. Raijmakers, C. R. Berkers, A. de Jong, H. Ovaa, A. J. Heck and S. Mohammed, *Mol. Cell. Proteomics*, 2008, **7**, 1755–1762.
30 D. L. Swaney, G. C. McAlister and J. J. Coon, *Nat. Methods*, 2008, **5**, 959–964.
31 D. L. Swaney, G. C. McAlister, M. Wirtala, J. C. Schwartz, J. E. Syka and J. J. Coon, *Anal. Chem.*, 2007, **79**, 477–485.
32 T. Taus, T. Kocher, P. Pichler, C. Paschke, A. Schmidt, C. Henrich and K. Mechtler, *J. Proteome Res.*, 2011, **10**, 5354–5362.
33 L. Kall, J. D. Canterbury, J. Weston, W. S. Noble and M. J. MacCoss, *Nat. Methods*, 2007, **4**, 923–925.
34 Y. Xue, J. Ren, X. Gao, C. Jin, L. Wen and X. Yao, *Mol. Cell. Proteomics*, 2008, **7**, 1598–1608.
35 Y. Xue, Z. Liu, J. Cao, Q. Ma, X. Gao, Q. Wang, C. Jin, Y. Zhou, L. Wen and J. Ren, *Protein Eng., Des. Sel.*, 2011, **24**, 255–260.
36 L. A. Pinna and M. Ruzzene, *Biochim. Biophys. Acta*, 1996, **1314**, 191–225.
37 N. Colaert, K. Helsens, L. Martens, J. Vandekerckhove and K. Gevaert, *Nat. Methods*, 2009, **6**, 786–787.
38 D. Szklarczyk, A. Franceschini, M. Kuhn, M. Simonovic, A. Roth, P. Minguez, T. Doerks, M. Stark, J. Muller, P. Bork, L. J. Jensen and C. von Mering, *Nucleic Acids Res.*, 2011, **39**, D561–D568.
39 B. Snel, G. Lehmann, P. Bork and M. A. Huynen, *Nucleic Acids Res.*, 2000, **28**, 3442–3444.
40 M. E. Smoot, K. Ono, J. Ruscheinski, P. L. Wang and T. Ideker, *Bioinformatics*, 2011, **27**, 431–432.
41 W. Huang da, B. T. Sherman and R. A. Lempicki, *Nat. Protoc.*, 2009, **4**, 44–57.
42 W. Huang da, B. T. Sherman and R. A. Lempicki, *Nucleic Acids Res.*, 2009, **37**, 1–13.
43 A. F. Altelaar, C. K. Frese, C. Preisinger, M. L. Hennrich, A. W. Schram, H. T. Timmers, A. J. Heck and S. Mohammed, *J. Proteomics*, 2012, http://dx.doi.org/10.1016/j.jprot.2012.10.009.
44 R. Amanchy, B. Periaswamy, S. Mathivanan, R. Reddy, S. G. Tattikota and A. Pandey, *Nat. Biotechnol.*, 2007, **25**, 285–286.
45 H. Molina, D. M. Horn, N. Tang, S. Mathivanan and A. Pandey, *Proc. Natl. Acad. Sci. U. S. A.*, 2007, **104**, 2199–2204.
46 D. L. Swaney, C. D. Wenger, J. A. Thomson and J. J. Coon, *Proc. Natl. Acad. Sci. U. S. A.*, 2009, **106**, 995–1000.
47 B. Domon, B. Bodenmiller, C. Carapito, Z. Hao, A. Huehmer and R. Aebersold, *J. Proteome Res.*, 2009, **8**, 2633–2639.
48 M. Aguiar, W. Haas, S. A. Beausoleil, J. Rush and S. P. Gygi, *J. Proteome Res.*, 2010, **9**, 3103–3107.
49 J. Villen, S. A. Beausoleil and S. P. Gygi, *Proteomics*, 2008, **8**, 4444–4452.
50 P. J. Ulintz, A. K. Yocum, B. Bodenmiller, R. Aebersold, P. C. Andrews and A. I. Nesvizhskii, *J. Proteome Res.*, 2009, **8**, 887–899.
51 M. M. Rinschen, M. J. Yu, G. Wang, E. S. Boja, J. D. Hoffert, T. Pisitkun and M. A. Knepper, *Proc. Natl. Acad. Sci. U. S. A.*, 2010, **107**, 3882–3887.
52 R. C. Hewer, G. B. Sala-Newby, Y. J. Wu, A. C. Newby and M. Bond, *J. Mol. Cell Cardiol.*, 2011, **50**, 87–98.
53 D. Hochbaum, K. Hong, G. Barila, F. Ribeiro-Neto and D. L. Altschuler, *J. Biol. Chem.*, 2008, **283**, 4464–4468.
54 M. Grandoch, A. Rose, M. ter Braak, V. Jendrossek, H. Rubben, J. W. Fischer, M. Schmidt and A. A. Weber, *Br. J. Cancer*, 2009, **101**, 2038–2042.
55 S. Haag, M. Warnken, U. R. Juergens and K. Racke, *Naunyn–Schmiedeberg's Arch Pharmacol.*, 2008, **378**, 617–630.
56 K. M. Kassel, T. A. Wyatt, R. A. Panettieri, Jr. and M. L. Toews, *Am. J. Physiol.*, 2008, **294**, L131–138.
57 H. Yan, D. A. Deshpande, A. M. Misior, M. C. Miles, H. Saxena, E. C. Riemer, R. M. Pascual, R. A. Panettieri and R. B. Penn, *FASEB J.*, 2011, **25**, 389–397.
58 N. Dube, M. R. Kooistra, W. J. Pannekoek, M. J. Vliem, V. Oorschot, J. Klumperman, H. Rehmann and J. L. Bos, *Cell. Signalling*, 2008, **20**, 1608–1615.
59 S. Krugmann, R. Williams, L. Stephens and P. T. Hawkins, *Curr. Biol.*, 2004, **14**, 1380–1384.
60 T. Yamada, T. Sakisaka, S. Hisata, T. Baba and Y. Takai, *J. Biol. Chem.*, 2005, **280**, 33026–33034.
61 B. Geiger, K. T. Tokuyasu, A. H. Dutton and S. J. Singer, *Proc. Natl. Acad. Sci. U. S. A.*, 1980, **77**, 4127–4131.
62 M. Reinhard, M. Halbrugge, U. Scheer, C. Wiegand, B. M. Jockusch and U. Walter, *EMBO J.*, 1992, **11**, 2063–2070.
63 V. Vasioukhin, C. Bauer, M. Yin and E. Fuchs, *Cell*, 2000, **100**, 209–219.
64 J. T. Parsons, A. R. Horwitz and M. A. Schwartz, *Nat. Rev. Mol. Cell Biol.*, 2010, **11**, 633–643.
65 E. M. Lafuente, A. A. van Puijenbroek, M. Krause, C. V. Carman, G. J. Freeman, A. Berezovskaya, E. Constantine, T. A. Springer, F. B. Gertler and V. A. Boussiotis, *Dev. Cell*, 2004, **7**, 585–595.
66 H. S. Lee, C. J. Lim, W. Puzon-McLaughlin, S. J. Shattil and M. H. Ginsberg, *J. Biol. Chem.*, 2009, **284**, 5119–5127.
67 N. Machida, M. Umikawa, K. Takei, N. Sakima, B. E. Myagmar, K. Taira, H. Uezato, Y. Ogawa and K. Kariya, *J. Biol. Chem.*, 2004, **279**, 15711–15714.

68 K. Taira, M. Umikawa, K. Takei, B. E. Myagmar, M. Shinzato, N. Machida, H. Uezato, S. Nonaka and K. Kariya, *J. Biol. Chem.*, 2004, **279**, 49488–49496.
69 H. Nonaka, K. Takei, M. Umikawa, M. Oshiro, K. Kuninaka, M. Bayarjargal, T. Asato, Y. Yamashiro, Y. Uechi, S. Endo, T. Suzuki and K. Kariya, *Biochem. Biophys. Res. Commun.*, 2008, **377**, 573–578.
70 P. J. Stork and J. M. Schmitt, *Trends Cell Biol.*, 2002, **12**, 258–266.
71 J. L. Bos, K. de Bruyn, J. Enserink, B. Kuiperij, S. Rangarajan, H. Rehmann, J. Riedl, J. de Rooij, F. van Mansfeld and F. Zwartkruis, *Biochem. Soc. Trans.*, 2003, **31**, 83–86.
72 J. V. Olsen, B. Blagoev, F. Gnad, B. Macek, C. Kumar, P. Mortensen and M. Mann, *Cell*, 2006, **127**, 635–648.
73 Y. Yu, S. O. Yoon, G. Poulogiannis, Q. Yang, X. M. Ma, J. Villen, N. Kubica, G. R. Hoffman, L. C. Cantley, S. P. Gygi and J. Blenis, *Science*, 2011, **332**, 1322–1326.
74 P. P. Hsu, S. A. Kang, J. Rameseder, Y. Zhang, K. A. Ottina, D. Lim, T. R. Peterson, Y. Choi, N. S. Gray, M. B. Yaffe, J. A. Marto and D. M. Sabatini, *Science*, 2011, **332**, 1317–1322.
75 C. Pan, J. V. Olsen, H. Daub and M. Mann, *Mol. Cell. Proteomics*, 2009, **8**, 2796–2808.
76 K. T. Rigbolt, T. A. Prokhorova, V. Akimov, J. Henningsen, P. T. Johansen, I. Kratchmarova, M. Kassem, M. Mann, J. V. Olsen and B. Blagoev, *Sci. Signaling*, 2011, **4**, rs3.